

Comparison of JET AVDE disruption data with M3D simulations and implications for ITER

*Original*

Comparison of JET AVDE disruption data with M3D simulations and implications for ITER / Strauss, H.; Joffrin, E.; Riccardo, V.; Breslau, J.; Paccagnella, R.; Subba, F.. - In: PHYSICS OF PLASMAS. - ISSN 1070-664X. - 24:10(2017). [10.1063/1.5004692]

*Availability:*

This version is available at: 11583/2986899 since: 2024-03-12T17:40:00Z

*Publisher:*

AIP Publishing

*Published*

DOI:10.1063/1.5004692

*Terms of use:*

This article is made available under terms and conditions as specified in the corresponding bibliographic description in the repository

*Publisher copyright*

(Article begins on next page)

## Comparison of JET AVDE disruption data with M3D simulations and implications for ITER

H. Strauss,<sup>1, a)</sup> E. Joffrin,<sup>2</sup> V. Riccardo,<sup>3</sup> J. Breslau,<sup>3</sup> R. Paccagnella,<sup>4</sup> and JET Contributors<sup>b)</sup>

<sup>1)</sup> *HRS Fusion, West Orange NJ 07052 USA*

<sup>2)</sup> *CEA, IRFM, F-13108 Saint-Paul-lez-Durance, France*

<sup>3)</sup> *Princeton Plasma Physics Laboratory, Princeton NJ 08570 USA*

<sup>4)</sup> *Consorzio RFX and Istituto Gas Ionizzati del C.N.R., 35127 Padua, Italy*

Nonlinear 3D MHD asymmetric vertical displacement disruptions simulations have been performed using JET equilibrium reconstruction initial data. Several experimentally measured quantities are compared with the simulation. These include vertical displacement, halo current, toroidal current asymmetry, and toroidal rotation. The experimental data and the simulations are in reasonable agreement. Also compared was the correlation of the toroidal current asymmetry and the vertical displacement asymmetry. The Noll relation between asymmetric wall force and vertical current moment is verified in the simulations. Also verified is toroidal flux asymmetry. Although in many ways JET is a good predictor of ITER disruption behavior, JET and ITER can be in different parameter regimes, and extrapolating from JET data can overestimate the ITER wall force.

PACS numbers: 52.55Fa, 52.55Tn, 52.65Kj

<sup>a)</sup> Electronic mail: [hank@hrsfusion.com](mailto:hank@hrsfusion.com)

<sup>b)</sup> See the author list of Overview of the JET results in support to ITER by X. Litaudon et al. to be published in Nuclear Fusion Special issue: overview and summary reports from the 26th Fusion Energy Conference (Kyoto, Japan, 17-22 October 2016)

## I. INTRODUCTION

A main source of predictions about ITER<sup>1</sup> disruptions is JET experimental data<sup>2</sup>. Further predictions have been made using MHD simulations<sup>3-7</sup>. Numerous other studies have been carried out, for example<sup>8-14</sup>. It is important to verify that the simulations are in agreement with JET data. This paper compares experimental data to MHD asymmetric vertical displacement event (AVDE) disruption simulations using the M3D<sup>15</sup> code.

It will also be pointed out in what sense JET is not a good predictor of ITER. JET and ITER can be in different parameter regimes. Although dimensional analysis indicates ITER asymmetric wall force could be 25 times larger than in JET<sup>2</sup>, the simulations presented in this paper show a novel result, that the ITER wall force might not be much larger than in JET.

The M3D simulations were initialized with EFIT equilibrium reconstruction of JET disruption shot 71985 at  $t = 67.3128s$ , with magnetic field  $B = 2T$ <sup>16,17</sup>, with carbon wall.

Detailed comparison of JET data with 3D MHD simulations has not been done previously. Several variables were compared in simulation and experiment and are in reasonable agreement. These include the time history of vertical position and current, halo current, asymmetric wall force, and toroidal rotation. Also compared was the correlation of the toroidal current asymmetry and the vertical displacement asymmetry, and a new analysis was provided. Toroidal flux asymmetry<sup>16</sup> was verified in the simulations. It is verified that the Noll relation<sup>18,19</sup> between asymmetric wall force and vertical current moment holds in the simulations. The comparison of JET data with 3D MHD simulation provides a validation of the M3D code.

The results obtained for the selected shot can be expected to be generally relevant to JET. The values of the compared quantities in this shot are typical of JET disruption data<sup>2</sup>.

The simulation parameters were Lundquist number  $S = 10^6$ , and the resistive wall Lundquist number was  $S_{wall} = \tau_{wall}/\tau_A = 250 - 1000$ , where  $\tau_{wall} = \mu_0 a \delta / \eta_{wall}$  is the wall magnetic field penetration time ( $a$  being the minor plasma radius,  $\delta$  the wall thickness, and  $\eta_{wall}$  the wall resistivity), and where  $\tau_A = R/v_A$  is the Alfvén time, with  $v_A$  the Alfvén speed and  $R$  the major radius. The simulation uses time units of  $\tau_A$ .

An important feature of the simulations is that most of the measured quantities are independent of simulational value of  $S_{wall}$ , for a given experimental wall time. This allows simulations to be run for much shorter times than when the experimental  $S_{wall}$  is used.

In the experiment, prior to the thermal quench (TQ),  $S = 10^9$ , but after the TQ,  $S \approx 10^5$ . The wall Lundquist number is  $S_{wall} = 7 \times 10^3$ .

The present simulations, both the TQ and the current quench (CQ) were included.

Section II describes the simulations and experimental data, Section III deals with comparison of halo current data, Section IV describes toroidal current and toroidal flux variation, Section V is concerned with the correlation of the toroidal variation of the toroidal current and the vertical displacement. Section VI discusses the Noll relation, Section VII describes toroidal rotation, Section VIII explains the asymmetric force to be expected in ITER, and finally Section IX summarizes the results.

## II. JET AVDE DISRUPTION SIMULATIONS AND EXPERIMENTAL MEASUREMENTS

The time history of the experimental data and simulation of shot 71985 are shown in Fig.1. The experimental toroidal current is denoted  $I_p$ , in  $MA$  and the vertical displacement as  $z_p$ . Time is in units of resistive wall time  $\tau_{wall}$ , which in the experiment is  $\tau_{wall}^{JET} = 0.005s^{20,21}$ . The simulated current  $I$  was driven according to the experimental current  $I_p$  in time normalized to the resistive wall time, with

$$I(t/\tau_{wall}) \propto I_p(t/\tau_{wall}^{JET}), \quad (1)$$

using the experimental time history data  $I_p(t)$  for shot 71985. Here  $\tau_{wall}$  is the resistive wall time in the simulation, which is less than the experimental resistive wall time. This rescaling was necessary because of computation time limitations on the simulations. As will be shown, the results are not strongly dependent on the choice of simulational  $\tau_{wall}$ . An artificial electric field current controller was applied to sustain the current, which keeps the simulation current approximately equal to the experimental current. Shown in Fig.1 are simulation total current  $I$  and vertical displacement  $\xi$ , and the experimental measurements of  $I_p$  and  $z_p$ , where  $I$ ,  $I_p$  are in  $MA$  and  $z_p, \xi$  are in  $m$ . The experimental data is presented

in units of experimental wall time, and the simulation is in units of simulation wall time. It is noteworthy that the simulated vertical displacement  $\xi$  agrees well with  $z_p$  during the growth and initial saturation phases. This agreement holds for all values of  $S_{wall}$  that were simulated.

The initial equilibrium obtained from the equilibrium reconstruction has  $q_0 < 1$ , which was unstable to a helical MHD instability with poloidal and toroidal mode numbers  $(m, n) = (1, 1)$  mode. This mode and the  $(1, 0)$  vertical instability combine to produce the TQ by  $t = 1.5\tau_{wall}$ .

Fig.2 shows contour plots in a simulation with  $S_{wall} = 1000$ , at time  $t = 3.93\tau_{wall}$  when the VDE has saturated, in the  $(R, Z)$  plane with  $\phi = 0$ . Fig.2(a) shows contours of poloidal magnetic flux  $\psi$ . Fig.2(b) shows the toroidal current density  $RJ_\phi$ , with a large  $(m, n) = (1, 1)$  internal kink perturbation. Fig.2(c) shows the toroidal magnetic field multiplied by  $R$ ,  $RB_\phi$ .

### III. HALO CURRENT

Fig.2(d) shows the toroidal field perturbation multiplied by  $R$ ,  $R\delta B_\phi$ , on the wall, at the same time as in Fig.2(a),(b),(c). The vertical coordinate is the toroidal angle  $\phi/(2\pi)$ , and the horizontal coordinate is a poloidal angle  $\theta/2\pi$ . The magnetic perturbation is largest along the line of the observation angle  $\theta_o \approx 2\pi/3$ , at the top of the JET wall, near the typical VDE strike point. Here

$$\delta B_\phi = B_\phi(\theta_o, t) - B_\phi(\theta_o, 0) \quad (2)$$

the difference between the flux at the observation angle  $\theta_o$  at times  $t = 3.93\tau_{wall}$  and  $t = 0$ .

Halo current is the current which flows on open field lines. In JET toroidal field measurements serve as a proxy for halo current<sup>17</sup>

$$I_{halo}^{JET} = 2\pi R\delta B_\phi \quad (3)$$

where  $\delta B_\phi$  is defined in (2).

Fig.2(d) has the largest flux perturbations at the observation angle. The JET halo current detectors measure toroidal magnetic field perturbations  $\delta B_\phi$  at  $\theta_o$  and at toroidal measurement angles  $\phi \approx (k - 1)\pi/2$ , with  $k = 1, \dots, 4$ . The JET torus is divided into octants, in

which toroidal field pick-up coils and Rogowskii coils are installed<sup>2,17</sup>. The halo current measurements are made in octants 1, 3, 5, 7.

In the following several quantities will be compared in simulation and experiment. Consider the variable  $f = f_0 + f_s \sin \phi + f_c \cos \phi$ . Listed are definitions of the average of  $f$  and the amplitude of the toroidally varying part of  $f$ ,

$$\begin{aligned}
 f &= \bar{f} + \tilde{f} \\
 \tilde{f} &= f - \bar{f} = f_s \sin \phi + f_c \cos \phi \\
 f_c &= \frac{1}{2}(f_5 - f_1) \\
 f_s &= \frac{1}{2}(f_7 - f_3) \\
 \bar{f} &= \oint f \frac{d\phi}{2\pi} = f_0 = \frac{1}{4}(f_1 + f_3 + f_5 + f_7) \\
 \Delta f &= \left( \oint \tilde{f}^2 \frac{d\phi}{\pi} \right)^{1/2} = (f_s^2 + f_c^2)^{1/2} = \frac{1}{2} [(f_5 - f_1)^2 + (f_7 - f_3)^2]^{1/2} \quad (4)
 \end{aligned}$$

Equivalent definitions are given for the case when  $f$  is represented as a Fourier series with  $n = 0$  and  $n = 1$  components, as in the simulations, or as a discrete set of values on four octants of a torus, as in the experiment.

Here  $\overline{\delta B}$  is the average of  $\delta B_\phi$  over the toroidal angles, and  $\Delta(\delta B)$  is the amplitude of the toroidally varying part. The simulated values were calculated by taking Fourier components of  $\delta B_\phi(\phi)$ . In Fig.3 these values are plotted as halo current fractions

$$\begin{aligned}
 HF_a &= 2\pi R \frac{\overline{\delta B}_a}{I_o} \\
 \Delta HF_a &= 2\pi R \frac{\Delta(\delta B)_a}{I_o} \quad (5)
 \end{aligned}$$

for the experimental ( $a = \text{exp}$ ) and simulated values ( $a = \text{sim}$ ) in units of experimental and simulational wall time respectively. Here  $I_o$  is the toroidal current at time  $t = 0$ . In the simulation,  $S_{wall} = 1000$ . The magnitudes of the peak values are in reasonable agreement.

The simulations were done for several values of  $S_{wall}$ . Fig.3(b) shows the peak value in time of  $HF$  and  $\Delta HF$ . The simulated values appear to converge to the experimental values, which implies that the peak values of the simulated quantities do not depend on the wall time. This allows the results to be extrapolated to the experimental value of  $S_{wall} = 7 \times 10^3$ . At present, computational restrictions limit the simulations to smaller values of  $S_{wall}$ .

#### IV. TOROIDAL CURRENT AND TOROIDAL FLUX VARIATION

Toroidal  $n = 1$  variation of toroidal current was observed in JET<sup>2,16</sup>. The time history plot Fig.4 shows the magnitude of the toroidal current variation comparing JET and simulation.

The toroidal current asymmetry is  $\Delta I$ , as defined above in (4), where the current is

$$I = \int J_\phi d^2x. \quad (6)$$

The asymmetric toroidal current can be obtained from  $\nabla \cdot \mathbf{J} = 0$ , or in integral form,

$$\frac{\partial I}{\partial \phi} = - \oint R J_n dl = -I_{halo}^{3D} \quad (7)$$

where the poloidal current normal to the wall is

$$J_n = \frac{1}{R} \frac{\partial(RB_\phi)}{\partial l} - \frac{1}{R} \frac{\partial B_l}{\partial \phi} \quad (8)$$

and where  $dl$  is the length element, and  $B_l$  is the component of magnetic field tangent to the wall. The 3D halo current  $I_{halo}^{3D}$  in (7) gives the net inflow or outflow of normal current at a particular toroidal angle<sup>4</sup> and vanishes if the current is toroidally symmetric.

In Fig.4, the experimental dimensionless current is labelled  $\Delta I_p/I_p$ , and the simulated value is  $\Delta I/I$ . The same discrete expression was used for experimental and simulated values. The agreement of the peak values is acceptable. The amplitude of  $\Delta I/I$  decays more rapidly in time than the experimental data, when the total current is decaying. The current variation  $\Delta I$  depends on the amplitude of the kink mode, as shown in (18),(20). This suggests that the decrease of  $\Delta I$  is caused by stabilization of the kink. In turn this may be caused by decay of the total current  $I$ , which can raise the value of  $q$ . The different behavior if the simulation and the experiment may be due to the different values of  $S$ , which governs the rate of resistive decay. The fluctuations in the simulated  $\Delta I/I$  may be related to fluctuations in  $I_p$  and  $\xi, z_p$  in Fig.1.

Also shown in Fig.4 is the toroidally varying toroidal magnetic flux  $\Delta \Phi/\Phi$ , where  $\Phi$  is

$$\Phi = \int B_\phi d^2x, \quad (9)$$

and  $\Delta \Phi$  is obtained using (4).

The toroidal variation of toroidal flux<sup>16</sup> follows from  $\nabla \cdot \mathbf{B} = 0$ ,

$$\frac{\partial \Phi}{\partial \phi} = - \oint R B_n dl. \quad (10)$$

To estimate the ratio of current perturbations to flux perturbations in Fig.4, take  $J_n \approx -\partial B_\theta / (R \partial \phi)$ . Assuming an  $(m, n) = (1, 1)$  mode, then  $J_n \approx -\partial B_\theta / (r \partial \theta)$ . From approximate incompressibility (12) with large aspect ratio<sup>15</sup>,  $J_n \approx \partial B_r / \partial r \approx B_n / a$ . Then (7),(10) give  $\Delta I \approx \Delta \Phi / a$ . Also with  $J_\phi \approx B_\phi / (qR)$ , where  $q$  is the rotational transform  $q = aB / (RB_\theta)$ , then

$$\frac{\Delta \Phi}{\Phi} \approx \frac{a}{qR} \frac{\Delta I}{I} \quad (11)$$

with  $qR/a \approx 5$ .

## V. CORRELATION OF TOROIDAL CURRENT AND VERTICAL DISPLACEMENT ASYMMETRY

The toroidal variation of the current and of the vertical displacement are positively correlated. Fig.5 shows experimental time histories of toroidal current differences  $(I_5 - I_1)/I$  plotted as a function of vertical displacement differences  $Z_5 - Z_1$ , and  $(I_7 - I_3)/I$  plotted as a function of  $Z_7 - Z_3$ , where the subscript refers to toroidal octant. These quantities correspond to  $\cos \phi$  and  $\sin \phi$  components of  $I_p, Z_p$ . Fig.5 also contains simulated  $n = 1$  Fourier components  $I_{\cos}/I$  as a function of  $\xi_{\cos}$ , and  $I_{\sin}/I$  as a function of  $\xi_{\sin}$ , which are the  $\cos \phi$  and  $\sin \phi$  harmonics of current  $I$  and vertical displacement  $\xi$ . These quantities are positively correlated, indicating that the toroidal plasma current is higher at toroidal locations where the plasma position is closer to the wall<sup>2,6</sup>. This effect has been explained by invoking skin current at the edge of the plasma<sup>2,10</sup>.

It can be shown analytically that the toroidal variation of current and vertical displacement are positively correlated. The maximum current occurs where the vertical displacement is also a maximum. The magnetic field in a large aspect ratio approximation is given by<sup>15</sup>

$$\mathbf{B} = \nabla \psi \times \hat{\phi} + B \hat{\phi} \quad (12)$$

and the displacement is

$$\xi = \nabla \chi \times \hat{\phi}. \quad (13)$$



The magnetic potential  $\psi$  is

$$\psi = \psi_0 + \mathbf{B} \cdot \nabla \chi \quad (14)$$

where  $\psi_0$  is the initial poloidal flux, and  $\chi$  is the displacement potential<sup>6</sup> of the VDE,

$$\chi = \tilde{\chi}_1 + \tilde{\chi}_2, \quad \tilde{\chi}_1 = \chi_1 \cos \theta, \quad \tilde{\chi}_2 = \chi_2 \cos(\theta - \phi) \quad (15)$$

Then  $\psi$  can be calculated from (14), (15) as  $\psi = \psi_0 + \psi_1 + \psi_2 + \psi_3$  and  $\mathbf{B} = \mathbf{B}_0 + \mathbf{B}_1 + \mathbf{B}_2 + \mathbf{B}_3$  with  $\mathbf{B}_0 = \nabla \psi_0 \times \hat{\phi} + B \hat{\phi}$ , and  $\mathbf{B}_k = \nabla \psi_k \times \hat{\phi}$ , where  $k = 1, 2, 3$ . A cylindrical model will be used. The toroidal current is given by

$$I = \oint B_\theta a d\theta = - \oint \psi' d\theta \quad (16)$$

where  $I = I_0 + I_1 + I_2 + I_3$ , and the prime denotes a radial derivative. Only contributions to  $\psi$  that are independent of  $\theta$  contribute to  $I$ . It is also assumed<sup>6</sup> that  $\chi = \psi = 0$  at the wall, so that only radial derivatives of  $\chi, \psi$  will contribute to  $I$ .

In zero order,  $\psi_0$  is a function of radius  $r$  only. In first, second, and third order,

$$\begin{aligned} \psi_1 &= \mathbf{B}_0 \cdot \nabla \tilde{\chi}_1 = -\frac{B_{\theta 0}}{a} \chi_1 \sin \theta \\ \psi_2 &= \mathbf{B}_0 \cdot \nabla \tilde{\chi}_2 + \mathbf{B}_1 \cdot \nabla \tilde{\chi}_1 \\ &= -\frac{B_{\theta 0}}{a} \chi_2 (1 - q) \sin(\theta - \phi) - \frac{B_{\theta 0}}{a^2} \chi_1' \chi_1 \\ \psi_3 &= \mathbf{B}_1 \cdot \nabla \tilde{\chi}_2 + \mathbf{B}_2 \cdot \nabla \tilde{\chi}_1 = -\frac{B_{\theta 0}}{a^2} (\chi_1 \chi_2)' (1 - \frac{q}{2}) \cos \phi \end{aligned} \quad (17)$$

and terms with  $\sin(2\theta), \cos(2\theta)$  were omitted because they do not contribute to  $I$ . The first and second order current vanishes,  $I_1 = I_2 = 0$ . The asymmetric current is given by

$$\frac{I_3}{2\pi} = -\psi_3' = (2 - q) \frac{B_{\theta 0}}{a^2} \chi_1' \chi_2' \cos \phi \quad (18)$$

This is compared to the asymmetric part of the displacement. The displacement in the  $\hat{y}$  direction is given by

$$\xi = \nabla(r \sin \theta) \times \nabla \chi \cdot \hat{\phi} = \xi_1 + \xi_2, \quad \xi_1 = -\frac{1}{2} \chi_1', \quad \xi_2 = -\frac{1}{2} \chi_2' \cos \phi \quad (19)$$

where  $\xi_1, \xi_2$  are the symmetric and asymmetric parts of the vertical displacement, respectively. The symmetric displacement is upward,  $\xi_1 > 0$ . The asymmetric  $\cos \phi$  terms have the

ratio

$$\frac{I_3}{\xi_2} = 4(2 - q) \frac{I_0 \xi_1}{a^2} \quad (20)$$

The ratio of current asymmetry  $I_3$  to the vertical displacement asymmetry  $\xi_2$  is positive, if  $q \leq 2$  at the wall.

In the experiment, simulations, and theory, toroidal plasma current is higher at toroidal locations where the plasma position is closer to the wall. There is no need to invoke skin currents<sup>2,10</sup>, which are not seen in the M3D simulations, to explain this effect.

## VI. NOLL RELATION OF $F_x$ AND $M_{IZ}$

The Noll relation is used in JET to estimate the asymmetric wall force<sup>19</sup>. The wall force in the wall volume is<sup>3,7</sup>

$$\mathbf{F}_{wall} = \delta_{wall} \oint \oint d\phi dl R \mathbf{J}_{wall} \times \mathbf{B}_{wall} \quad (21)$$

where  $\delta_{wall}$  is the wall thickness,  $\mathbf{J}_{wall}$  is the wall current density, and  $\mathbf{B}_{wall}$  is the magnetic field in the wall. The projections of the toroidally varying wall force in the  $\hat{\mathbf{x}}, \hat{\mathbf{y}}$  directions are given by  $\tilde{F}_x = \mathbf{F} \cdot \hat{\mathbf{x}}, \tilde{F}_y = \mathbf{F} \cdot \hat{\mathbf{y}}$ . The magnitude of the asymmetric horizontal force is defined as

$$\Delta F_x = (\tilde{F}_x^2 + \tilde{F}_y^2)^{1/2}. \quad (22)$$

The asymmetric wall force is proportional to the asymmetric vertical current moment, which is given by

$$\Delta F_x \approx \pi B \Delta M_{IZ} \quad (23)$$

where

$$M_{IZ} = \int Z J_\phi d^2x \quad (24)$$

and the simulated and experimental  $\Delta M_{IZ}$  are calculated using (4). Fig.6(a) compares the wall force in the simulation with simulated and experimental vertical current moment.

The units are in  $MN$ . The asymmetric force maximum amplitude is  $\Delta F_x = 1.1MN$ . The experimental Noll formula predicts a force of  $1.3MN$ , while the simulated formula predicts  $1.2MN$ . The agreement is very good. Fig.6(b) shows the peak values in simulations with different values of  $S_{wall}$ . The agreement is essentially independent of  $S_{wall}$ .

## VII. TOROIDAL ROTATION

Asymmetric force rotation is of concern in ITER. Rotation is observed in both experiment and simulations. The rotation angle calculated from the experimental data is

$$\alpha_{exp} = \tan^{-1} \left( \frac{I_5 - I_1}{I_7 - I_3} \right) \quad (25)$$

The simulated rotation angle taken from the current was rather noisy, so the force angle

$$\alpha_{sim} = \tan^{-1} \left( \frac{\tilde{F}_y}{\tilde{F}_x} \right) \quad (26)$$

was used instead, where  $\tilde{F}_x, \tilde{F}_y$  are defined after (21). Fig.7(a) shows rotation angle  $\alpha$  in experiment and in a simulation with  $S_{wall} = 10^3$ . In both cases there are about  $N_{rot} = 2.8$  periods during the CQ time  $\tau_{CQ} = 5\tau_{wall}$ , which is the time interval of substantial halo current in Fig.1. In runs with  $S_{wall} = 250$  and  $S_{wall} = 500$ ,  $N_{rot} \approx 2.6$  and  $N_{rot} \approx 2.0$  respectively, as shown in Fig.7(b). Also shown in the experimental value  $N_{exp} = 2.8$ .

Fig.7(b) implies that the rotation frequency is  $f_{rot} = N_{rot}/\tau_{CQ} \approx (2S_{wall})^{-1}$ . This suggests the rotation is involved with the resistive wall interaction.

## VIII. IMPLICATIONS FOR ITER

In the experiment and simulations presented in the previous sections, the maximum wall force occurs after the vertical displacement saturates. In JET,  $\tau_{wall}^{JET} = 0.005s$ , and the experimental current quench time is  $\tau_{CQ}^{JET} \approx 5 \times \tau_{wall} \gg \tau_{wall}$ . This will be denoted the high  $\tau_{CQ}/\tau_{wall}$  regime.

There is a second, low  $\tau_{CQ}/\tau_{wall}$  regime, in which  $\tau_{CQ}/\tau_{wall} \lesssim 1$ , in which the asymmetric wall force and halo current are much smaller. To show this, the wall time was artificially increased, keeping the CQ time fixed. Fig.8 shows JET simulation time histories of  $I$  and  $\xi$ , with  $S_{wall} = 1000$ . The subscripts indicate different values of  $\tau_{CQ}/\tau_{wall} =$  (a) 1.67, (b) 1.25, (c) 0.83. These were obtained by multiplying  $\tau_{wall}^{JET}$  in (1), by (a) 3, (b) 4, and (c) 6, noting that in the simulations,  $\tau_{CQ}/\tau_{wall} = \tau_{CQ}^{JET}/\tau_{wall}^{JET}$ .

There is an interesting crossover in the behavior of  $\xi$ . For case (a),  $\xi$  saturates in a stationary state, similar to Fig.1. For cases (b),(c),  $\xi$  does not saturate, but grows to almost

the vertical height of the wall. Saturation of  $\xi$  seems to require  $\tau_{CQ}/\tau_{wall} \gtrsim 1.5$ . It is also noteworthy that a faster CQ causes a speedup of the VDE.

In Fig.9(a),(b), the ratio  $\tau_{CQ}/\tau_{wall}$  was varied by replacing the experimental wall time in (1) by a wider range of values,  $0.005 \leq \tau_{wall}^{JET} \leq 0.03$ . The cases in Fig.8 have the smallest  $\tau_{CQ}/\tau_{wall}$  and  $\Delta F_x$  values in Fig.9(a). From Fig.8 and Fig.9(a) it is possible to distinguish three regimes of  $\tau_{CQ}/\tau_{wall}$ . In the low  $\tau_{CQ}/\tau_{wall}$  regime  $\tau_{CQ}/\tau_{wall} \lesssim 1.5$ , the asymmetric wall force is small, while in the high  $\tau_{CQ}/\tau_{wall}$  regime  $\tau_{CQ}/\tau_{wall} \gtrsim 4$ ,  $\Delta F_x$  is large. There is also an intermediate regime  $1.5 \lesssim \tau_{CQ}/\tau_{wall} \lesssim 4$ .

A reason for this behavior is that a large force seems to require both a large vertical displacement and a large current. Fig.6(a) shows that the asymmetric wall force  $\Delta F_x$  is maximum when  $\xi$  and  $I$  are simultaneously near their maximum values in Fig.1. Fig.8 shows that in the low  $\tau_{CQ}/\tau_{wall}$  regime  $\xi$  and  $I$  do not simultaneously have their largest values.

The fit in Fig.9(a) is to

$$\Delta F_x = c_1 [1 + \tanh(c_2 \frac{\tau_{CQ}}{\tau_{wall}} - c_3)] \quad (27)$$

where  $c_1 = 1.1$ ,  $c_2 = 1$ , and  $c_3 = 2.7$ . The half maximum occurs when  $\tau_{CQ}/\tau_{wall} \approx 2.7$ .

Fig.9(a) also shows the dependence of the Noll formula (23) on  $\tau_{CQ}/\tau_{wall}$ . It is in agreement with  $\Delta F_x$ , in the high  $\tau_{CQ}/\tau_{wall}$  regime, but otherwise greatly exceeds the wall force. It suggests that (23) gives an upper limit to the asymmetric wall force. Here the fit is to (27) with  $\pi B \Delta M_{Iz}$  replacing  $\Delta F_x$ ,  $c_1 = 1.2$ ,  $c_2 = 0.9$ , and  $c_3 = 1.9$ .

Fig.9(b) shows the simulated toroidally averaged halo current  $HF$  and the toroidally varying halo current  $\Delta HF$  defined in (5) as a function of  $\tau_{CQ}/\tau_{wall}$ , as in Fig.9(b). The fits are to  $HF$ ,  $\Delta HF$  on the left side of (27), with  $c_1 = 0.17$ ,  $c_2 = 0.85$ ,  $c_3 = 1.3$ , and  $c_1 = 0.07$ ,  $c_2 = 1$ ,  $c_3 = 3$  respectively. A related ITER study<sup>14</sup> found that reducing  $\tau_{CQ}$  by mitigation reduced the halo current, by causing a CQ before the vertical displacement was large.

The low  $\tau_{CQ}/\tau_{wall}$  regime is the regime most relevant to ITER. The ITER wall time is much longer than in JET. The walls in ITER<sup>22</sup> have thickness  $\delta = 6cm$ , resistivity  $\eta = 0.825\mu\Omega m$ , and minor radius of the inner wall in the poloidal midplane  $a_1 = 1.35 \times a_p = 2.7m$

where  $a_p = 2m$  is the plasma minor radius. This gives the wall time  $\tau_{wall}^{ITER} = \mu_0 a_1 \delta / \eta = 0.26s$ . A mitigated CQ time might be  $0.05s - 0.15s^{9,23,24}$ . In a slow unmitigated ITER CQ,  $\tau_{CQ} \lesssim 0.3s^{24}$ . In these examples,  $\tau_{CQ}^{ITER} \leq \tau_{wall}^{ITER}$ . There might be slow<sup>24</sup> CQs with  $\tau_{CQ}^{ITER} \lesssim 0.6s$ .

It has been predicted that the asymmetric wall force in ITER might be 25 times as large as the wall force in JET<sup>2</sup>, which is a serious concern in the high  $\tau_{CQ}/\tau_{wall}$  regime.

The simulations suggest that the wall force in ITER will be much less in the low  $\tau_{CQ}/\tau_{wall}$  regime. If the wall force in the low  $\tau_{CQ}/\tau_{wall}$  regime is 4% of the maximum, then the scaling to ITER is  $25 \times 0.04 = 1$ , so that  $\Delta F_x$  might be the same in ITER as in JET.

Previous simulations of ITER disruptions<sup>3,4</sup> found a large variation in the amplitude of  $\Delta F_x$  which depended on  $\tau_{wall}$ . In some of the simulations<sup>4</sup>, a VDE caused magnetic flux to be scraped off, so that the last closed flux surface had  $q = 2$ . This caused a 3D MHD instability with growth rate  $\gamma$ , which produced a maximum asymmetric force if it saturated in about the wall time,  $\gamma\tau_{wall} = \mathcal{O}(1)$ . When the wall time was larger,  $\gamma\tau_{wall} \ll 1$ , the amplitude of asymmetric wall force was an order of magnitude less. Other simulations<sup>4</sup> modeled the effect of massive gas injection by concentrating the current within the  $q = 2$  surface. As in the present simulations, the 3D MHD instability was present before the VDE. An example was given in the low  $\tau_{CQ}/\tau_{wall}$  regime, with  $\Delta F_x$  less than 10% of the maximum value. In those previous simulations, the CQ was not controlled, and the scaling of  $\Delta F_x$  with  $\tau_{CQ}/\tau_{wall}$  was not studied systematically.

In order to confirm that the JET results in the low  $\tau_{CQ}/\tau_{wall}$  regime are applicable to ITER, it is important to perform simulations with ITER geometry and parameters, with control of the CQ, as in the present study. It is important to see if ITER is similar to cases (b), (c), in Fig.8, which have wall force much smaller than the maximum value, as shown in Fig.9(a).

## IX. SUMMARY

Nonlinear 3D MHD asymmetric vertical displacement disruptions simulations have been performed using JET equilibrium reconstruction initial data. Several experimentally mea-

sured quantities were compared with the simulation. It was found that there was reasonable agreement between simulation and experiment. The quantities that were compared were the VDE displacement and toroidal current, the halo current, the toroidal current asymmetry, and toroidal rotation. The experimental data and the simulations are in reasonable agreement. The toroidal current and vertical displacement asymmetry are positively correlated as in the experiment. It is not necessary to invoke skin current to explain the correlation. The Noll relation between asymmetric wall force and vertical current moment is verified in the simulations. Also verified is toroidal variation of toroidal magnetic flux. An important feature of the simulations is that most of the quantities are independent of  $S_{wall}$ , when the time is also scaled to  $S_{wall}$ . This allows simulations to be run for much shorter times than when the experimental  $S_{wall}$  is used. The values of the compared quantities in this JET shot are fairly typical of JET disruption data. In future work other experimental shots might be compared to simulations.

In JET, the wall time is much less than the current quench time,  $\tau_{wall} \ll \tau_{CQ}$ , which is the high  $\tau_{CQ}/\tau_{wall}$  regime. It was shown in JET simulations that there is also a low  $\tau_{CQ}/\tau_{wall}$  regime, in which  $\tau_{wall} \gtrsim \tau_{CQ}$ . In this regime the asymmetric wall force and halo current are much less than in the slow CQ regime. The low  $\tau_{CQ}/\tau_{wall}$  regime is more relevant to ITER. Extrapolating from JET data might greatly overestimate the expected ITER asymmetric wall force. It is important to carry out further ITER simulations to verify this conclusion.

**Acknowledgement:** We thank M. Lehnen for helpful comments. This research was supported by USDOE, has been carried out within the framework of the EUROfusion Consortium, and has received funding from the Euratom research and training programme 2014-2018 under grant agreement No 633053. The views and opinions expressed herein do not necessarily reflect those of the European Commission.

## REFERENCES

- <sup>1</sup>T. Hender, J. C. Wesley, J. Bialek, A. Bondeson, A. Boozer, R. J. Buttery, A. Garofalo, T. P. Goodman, R. S. Granetz, Y. Gribov, O. Gruber, M. Gryaznevich, G. Giruzzi, S. Günter, N. Hayashi, P. Helander, C. C. Hegna, D. F. Howell, D. A. Humphreys, G. T. A. Huysmans, A. W.

- Hyatt, A. Isayama, S. C. Jardin, Y. Kawano, A. Kellman, C. Kessel, H. R. Koslowski, R. J. La Haye, E. Lazzaro, Y. Q. Liu, V. Lukash, J. Manickam, S. Medvedev, V. Mertens, S. V. Mirnov, Y. Nakamura, G. Navratil, M. Okabayashi, T. Ozeki, R. Paccagnella, G. Pautasso, F. Porcelli, V. D. Pustovitov, V. Riccardo, M. Sato, O. Sauter, M. J. Schaffer, M. Shimada, P. Sonato, E. J. Strait, M. Sugihara, M. Takechi, A. D. Turnbull, E. Westerhof, D. G. Whyte, R. Yoshino, H. Zohm and the ITPA MHD, Disruption and Magnetic Control Topical Group, Nuclear Fusion **47** S128 - 202 (2007). Progress in the ITER Physics Basis Chapter 3: MHD Stability, operational limits and disruptions, Nuclear Fusion **47** (2007) S128 - S202.
- <sup>2</sup>S.N. Gerasimov, T.C. Hender, J. Morris, V. Riccardo, L.E. Zakharov and JET EFDA Contributors, Plasma current asymmetries during disruptions in JET, Nucl. Fusion **54** 073009 (2014).
- <sup>3</sup>H. R. Strauss, R. Paccagnella, J. Breslau, Wall forces produced during ITER disruptions, Phys. Plasmas (2010) **17**, 082505.
- <sup>4</sup>H. Strauss, R. Paccagnella, J. Breslau, L. Sugiyama, S. Jardin, Sideways Wall Force Produced During Disruptions, Nucl. Fusion **53**, 073018 (2013).
- <sup>5</sup>H. R. Strauss, L. Sugiyama, R. Paccagnella, J. Breslau, S. Jardin, Tokamak toroidal rotation caused by AVDEs and ELMs, Nuclear Fusion **54**, 043017 (2014).
- <sup>6</sup>H. Strauss, Toroidal current asymmetry in tokamak disruptions, Physics of Plasmas **21**, 102509 (2014).
- <sup>7</sup>H. Strauss, Asymmetric Wall Force and Toroidal Rotation in Tokamak Disruptions, Phys. Plasmas **22**, 082509 (2015).
- <sup>8</sup>V. A. Izzo, D. G. Whyte, R. S. Granetz, P. B. Parks, E. M. Hollmann, L. L. Lao, J. C. Wesley, Magnetohydrodynamic simulations of massive gas injection in Alcator C - Mod and DIII-D plasmas, Phys. Plasmas **15**, 056109 (2008).
- <sup>9</sup>E. M. Hollmann, P. B. Aleynikov, T. Flp, D. A. Humphreys, V. A. Izzo, M. Lehnen, V. E. Lukash, G. Papp, G. Pautasso, F. Saint-Laurent, and J. A. Snipes, Status of research toward the ITER disruption mitigation system, Phys. Plasmas **22**, 021802 (2015).
- <sup>10</sup>L. E. Zakharov, The theory of the kink mode during the vertical plasma disruption events in tokamaks, Phys. Plasmas **15** 062507 (2008).

- <sup>11</sup>L. E. Zakharov, Sergei A. Galkin, Sergei N. Gerasimov, and JET-EFDA contributors, Understanding disruptions in tokamaks, *Phys. Plasmas* **19** 055703 (2012).
- <sup>12</sup>R. Roccella, M. Roccella, V. Riccardo, S. Chiochio and JET Contributors, Asymmetric toroidal eddy currents (ATEC) to explain sideways forces at JET Nuclear Fusion **56** 106010 (2016).
- <sup>13</sup>R. R. Khayrutdinov, V. E. Lukash, V. D. Pustovitov, Local and integral forces on the vacuum vessel during thermal quench in the ITER tokamak Plasma Physics and Controlled Fusion **58** 115012 (2016).
- <sup>14</sup>M. Sugihara, S. Putvinski, D. J. Campbell, S. Carpentier-Chouchana, F. Escourbiac, S. Gerasimov, Yu. Gribov, T. C. Hender, T. Hirai, K. Ioki, R. Khayrutdinov, H. Labidi, V. Lukash, S. Maruyama, M. Merola, R. Mitteau, S. Miyamoto, J. Morris, G. Pautasso, R. A. Pitts, R. Raffray, V. Riccardo, R. Roccella, G. Sannazzaro, T. Schioler, J. Snipes, R. Yoshino Disruption Impacts and Their Mitigation Target Values for ITER Operation and Machine Protection, ITR/P1-14, IAEA Fusion Energy Conference 2012, San Diego.
- <sup>15</sup>W. Park, E. Belova, G. Y. Fu, X. Tang, H. R. Strauss, L. E. Sugiyama, Plasma Simulation Studies using Multilevel Physics Models, *Phys. Plasmas* **6** 1796 (1999).
- <sup>16</sup>S. N. Gerasimov, P. Abreu, M. Baruzzo, V. Drozdov, A. Dvornova, J. Havlicek, T.C. Hender, O. Hronova, U. Kruezi1, X. Li, T. Markovi, R. Pnek, G. Rubinacci, M. Tsalas, S. Ventre, F. Villone, L.E. Zakharov and JET Contributors JET and COMPASS asymmetrical disruptions, *Nucl. Fusion* **55** 113006 (2015).
- <sup>17</sup>V. Riccardo, G. Arnoux, P. Cahyna, T. C. Hender, A. Huber, S. Jachmich, V. Kiptily, R. Koslowski, L. Krln, M. Lehnen, A. Loarte, E. Nardon, R. Paprok, D. Tskhakaya (Sr) and JET-EFDA contributors JET disruption studies in support of ITER, *Plasma Phys. Contr. Fusion* **52**, (2010).
- <sup>18</sup>P. Noll, P. Andrew, M. Buzio, R. Litunovski, T. Raimondi, V. Riccardo, and M. Verrecchia, (Proc. 19th Symposium on Fusion Technology, Lisbon, 1996) ed. C. Varandas and F. Serra (Elsevier, Amsterdam, 1996), Vol. 1, p. 751.
- <sup>19</sup>V. Riccardo, P. Noll, S.P. Walker, Forces between plasma, vessel and TF coils during AVDEs at JET, *Nuclear Fusion* **40** 1805 (2000).



- <sup>20</sup>V. Riccardo, T. C. Hender, P. J. Lomas, B. Alper, T. Bolzonella, P. de Vries, G. P. Maddison and the JET EFDA Contributors, Analysis of JET halo currents, Plasma Phys. Control. Fusion **46**, 925 (2004).
- <sup>21</sup>R. Albanese, M. Mattei and F. Villone, Prediction of the growth rates of VDEs in JET, Nucl. Fusion **44**, 999 (2004).
- <sup>22</sup>Y. Gribov and V. D. Pustovitov, Analytical study of RWM feedback stabilisation with application to ITER, Proc. 19th IAEA Fusion Energy Conf. (Lyon, 2002) CT/P-12 [http://www-pub.iaea.org/MTCD/publications/PDF/csp\\_019c/pdf/ctp\\_12.pdf](http://www-pub.iaea.org/MTCD/publications/PDF/csp_019c/pdf/ctp_12.pdf)
- <sup>23</sup>M. Lehnen, Physics basis for ITER disruption mitigation gaps and present R&D, Theory and Simulation of Disruptions Workshop, Princeton, 20 July 2016, <http://tsdw.pppl.gov/Talks/2016/Lehnen.pdf>
- <sup>24</sup>D. Kiramov, M. Lehnen, R. Khayrutdinov, V. Lukash, ITER disruption simulations with improved power balance in the halo region, 43rd EPS Conference on Plasma Physics, P4.071 (2016), <http://ocs.ciemat.es/EPS2016PAP/pdf/P4.071.pdf>

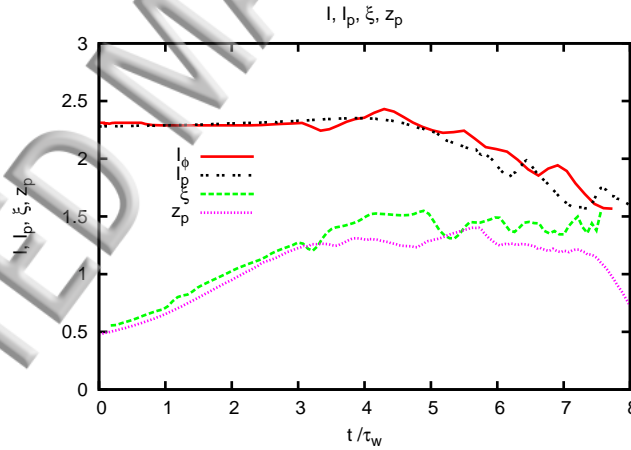


FIG. 1. Time history plot of simulated toroidal current  $I$ , experimental toroidal current  $I_p$ , simulated vertical displacement  $\xi$ , and experimental vertical displacement  $z_p$ . Simulation quantities are in time units  $\tau_{wall} = S_{wall}\tau_A$ , with  $S_{wall} = 1000$ . Experimental quantities are in time units

$\tau_{wall}^{JET}$ .

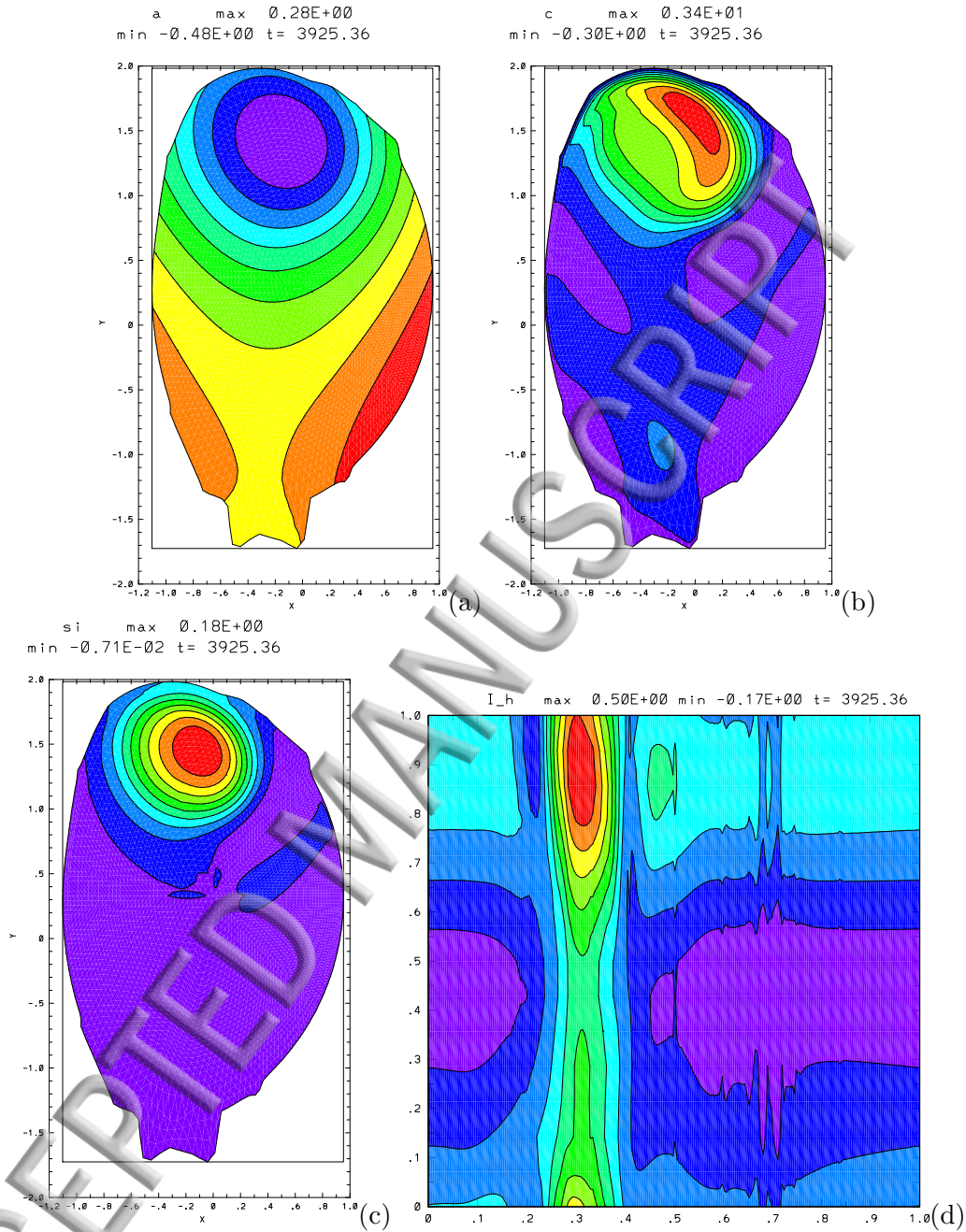


FIG. 2. (a) Contour plot of poloidal magnetic flux  $\psi$  at time  $t = 3.93\tau_{wall}$  in the  $(R, Z)$  plane with  $\phi = 0$ , with  $S_{wall} = 1000$ , when the vertical displacement has saturated. (b) Contours of toroidal current at the same time. A large  $(m, n) = (1, 1)$  mode is present. (c) Contours of toroidal magnetic flux  $RB_\phi$ . (d) Perturbed toroidal field on the wall,  $R\delta B_\phi$  at the same time. The vertical coordinate is the toroidal angle  $\phi/(2\pi)$ , and the horizontal coordinate is a poloidal angle  $\theta/2\pi$ .

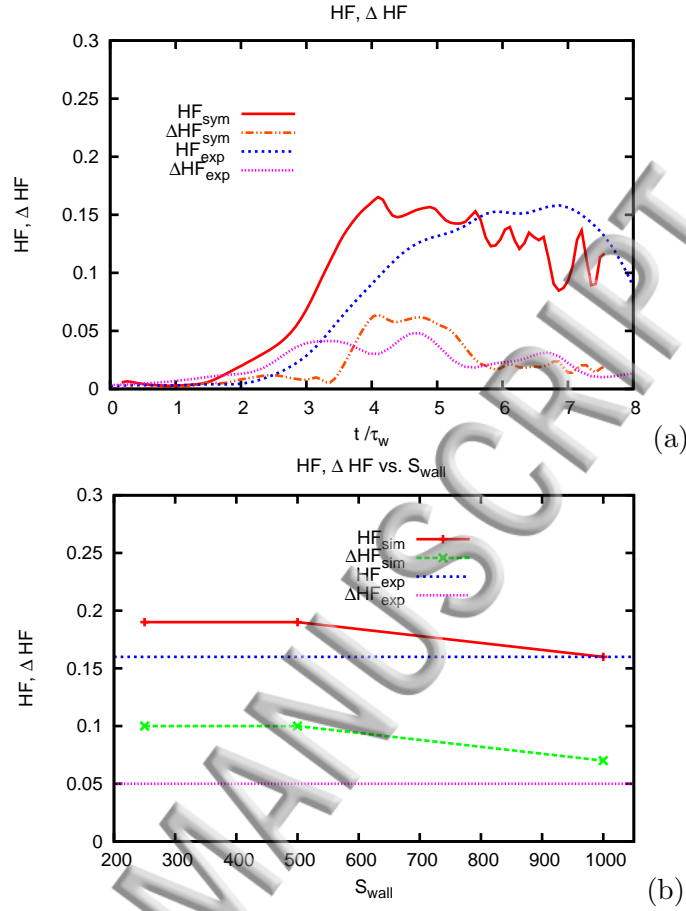


FIG. 3. (a) Time history of toroidally averaged experimental halo current  $HF_{exp}$ , toroidally varying experimental halo current  $\Delta HF_{exp}$ , toroidally averaged simulated halo current  $HF_{sim}$ , and toroidally varying simulated halo current  $\Delta HF_{sim}$ , defined in (5) with simulation  $S_{wall} = 1000$ . (b) Maximum values in time of toroidally averaged  $HF$  and varying  $\Delta HF$ , both simulated and experimental, as a function of  $S_{wall}$ .

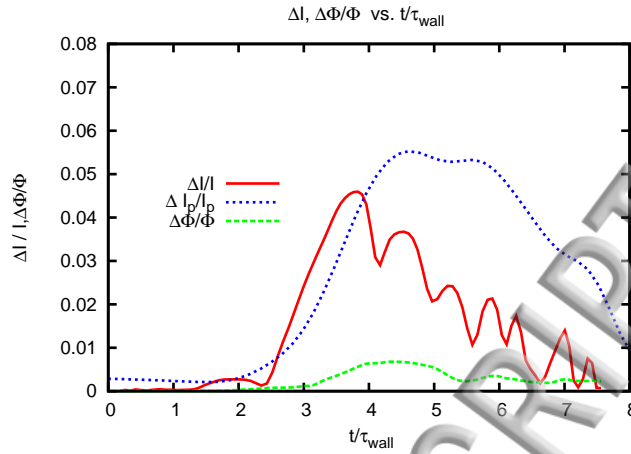


FIG. 4. Time history plot shows magnitude of toroidal current variation comparing JET data  $\Delta I_p/I_p$  and simulation  $\Delta I/I$ . Also shown is the toroidally varying toroidal flux amplitude  $\Delta\Phi/\Phi$ .

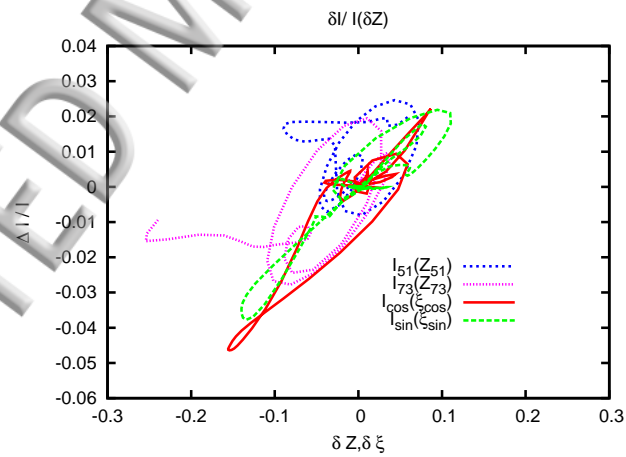


FIG. 5. Time history of toroidal current differences  $\delta I/I$  as a function of vertical displacement differences  $\delta\xi, \delta z_p$ , in experiment and simulation.

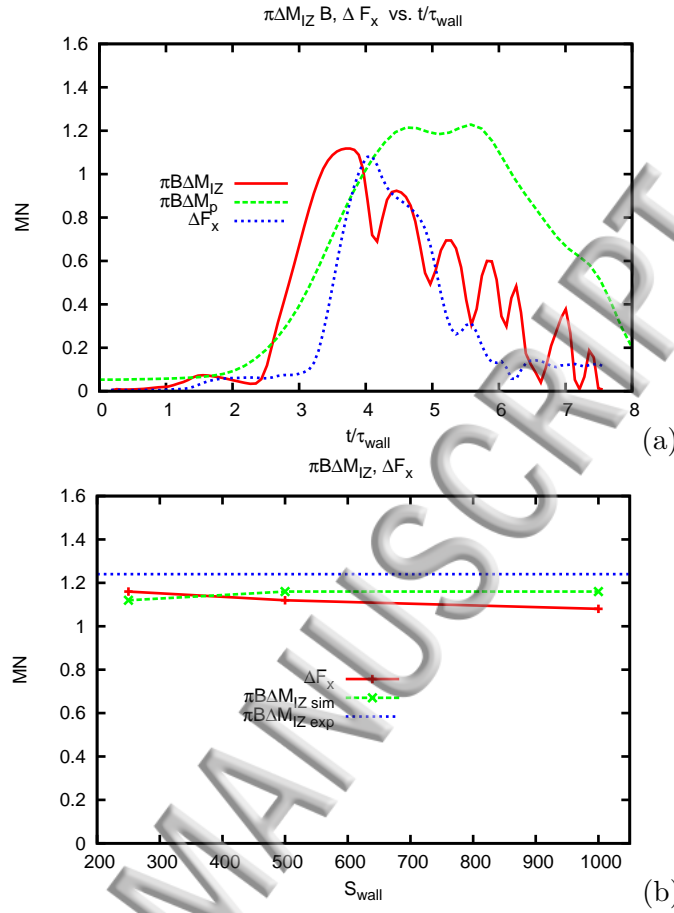


FIG. 6. (a) Simulated asymmetric wall force  $\Delta F_x$  is consistent with the Noll formula, which is calculated both from the simulation  $\Delta M_{Iz sim}$  and the experimental data  $\Delta M_{Iz exp}$ . (b) Peak values are in agreement, essentially independent of  $S_{wall}$ . The units are  $MN$ .

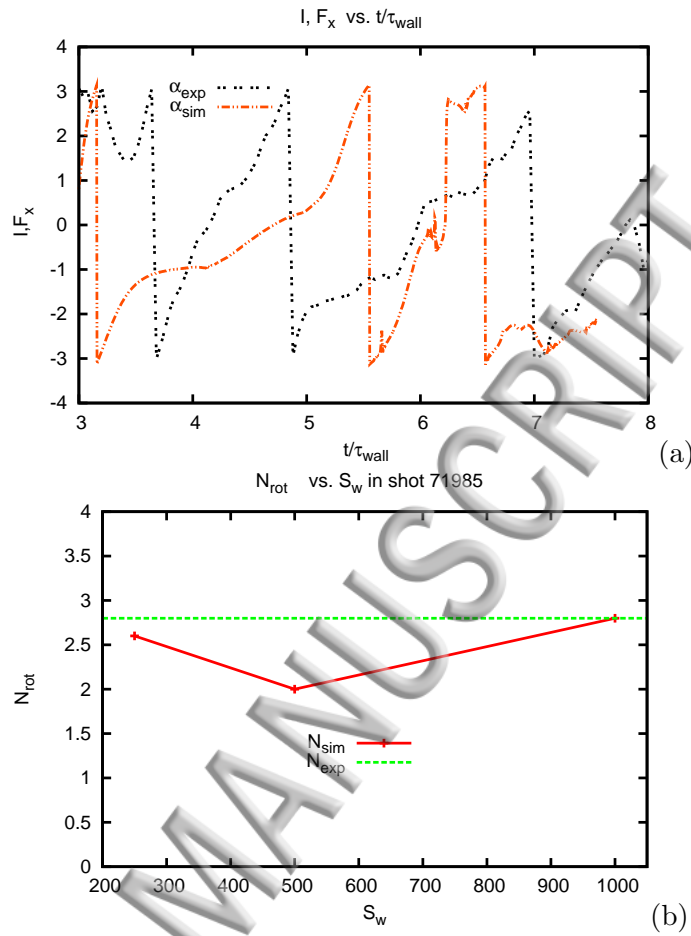


FIG. 7. Rotation of toroidal current and wall force. (a) wall force angle in wall time units, for  $S_{wall} = 10^3$ . Also shown is the experimental current rotation angle. (b) Rotation number  $N_{rot} = (\alpha_F - \alpha_i)/(2\pi)$  as a function of  $S_{wall}$ . Also shown is the experimental value of  $N_{rot}$  taken from Fig.7(a).

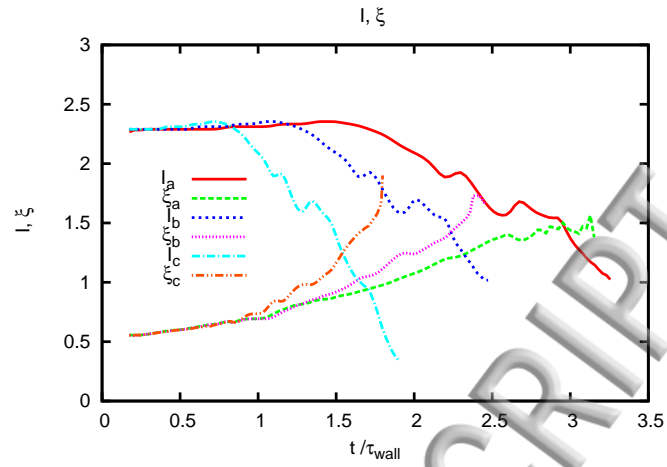


FIG. 8. Time histories of  $I$ ,  $\xi$  as in Fig.1, with  $S_{wall} = 1000$ . Subscripts denote values of  $\tau_{CQ}/\tau_{wall} =$  (a) 1.67, (b) 1.25, (c) 0.83. In case (a)  $\xi$  saturates in a steady state, while in (b) , (c)  $\xi$  does not saturate.

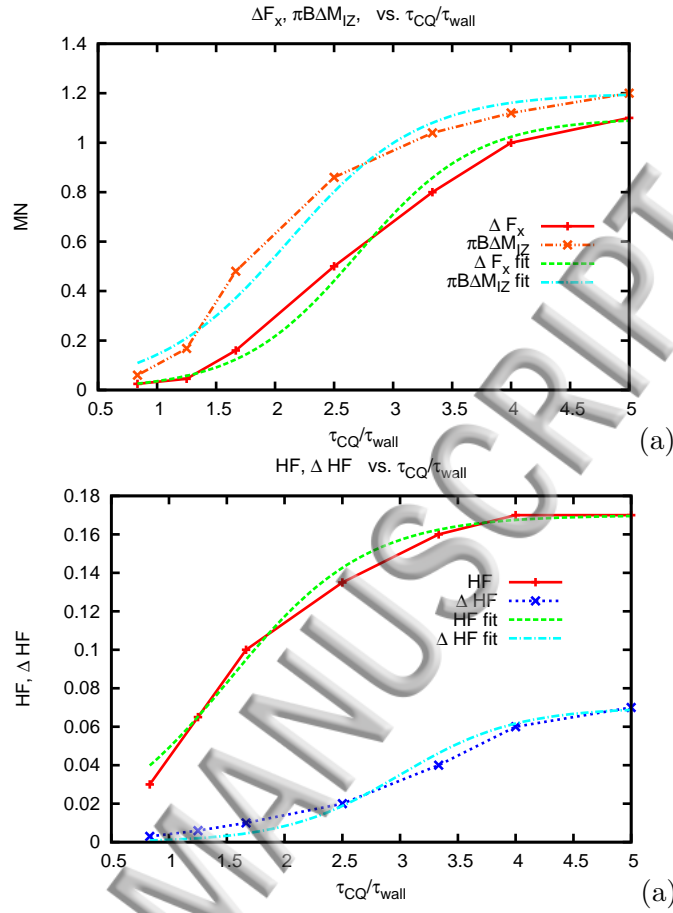
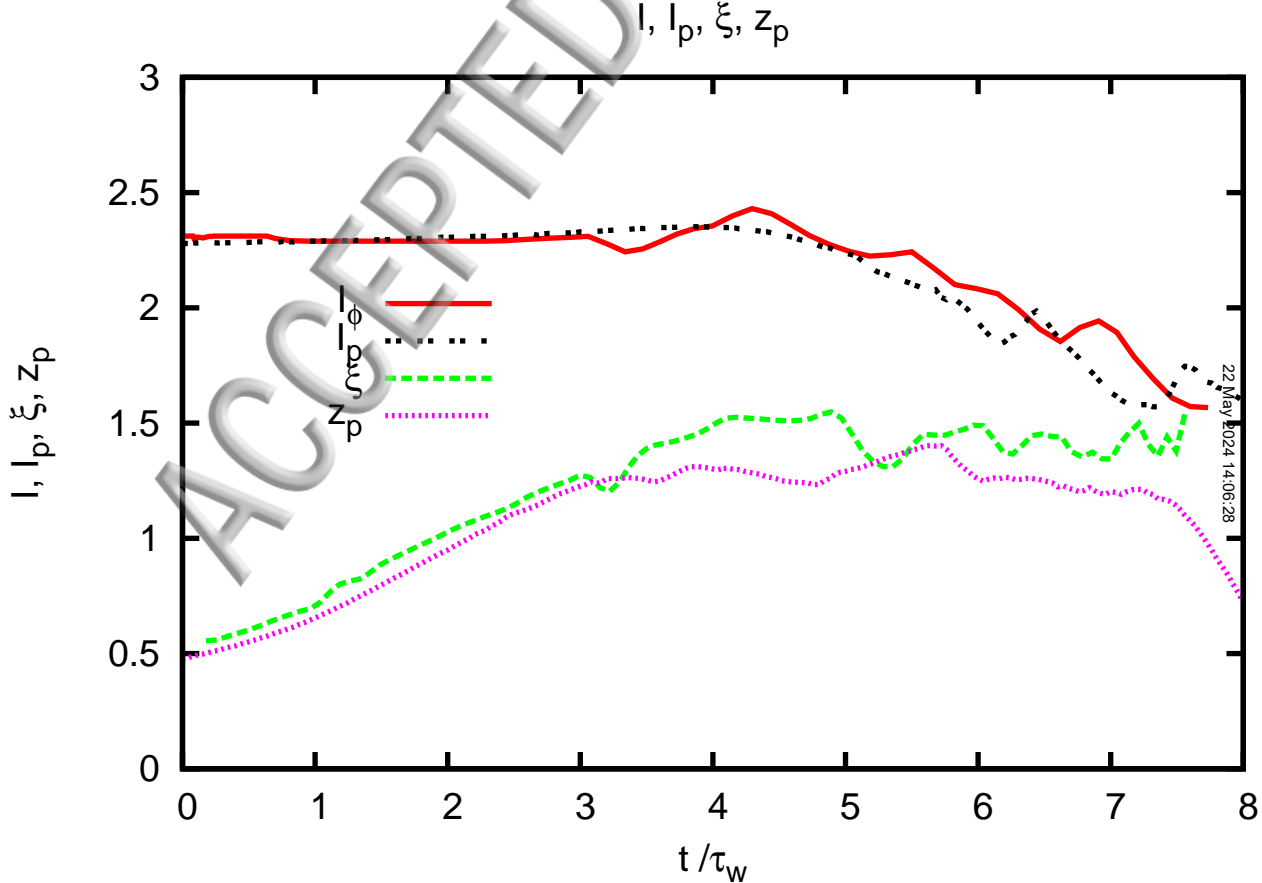
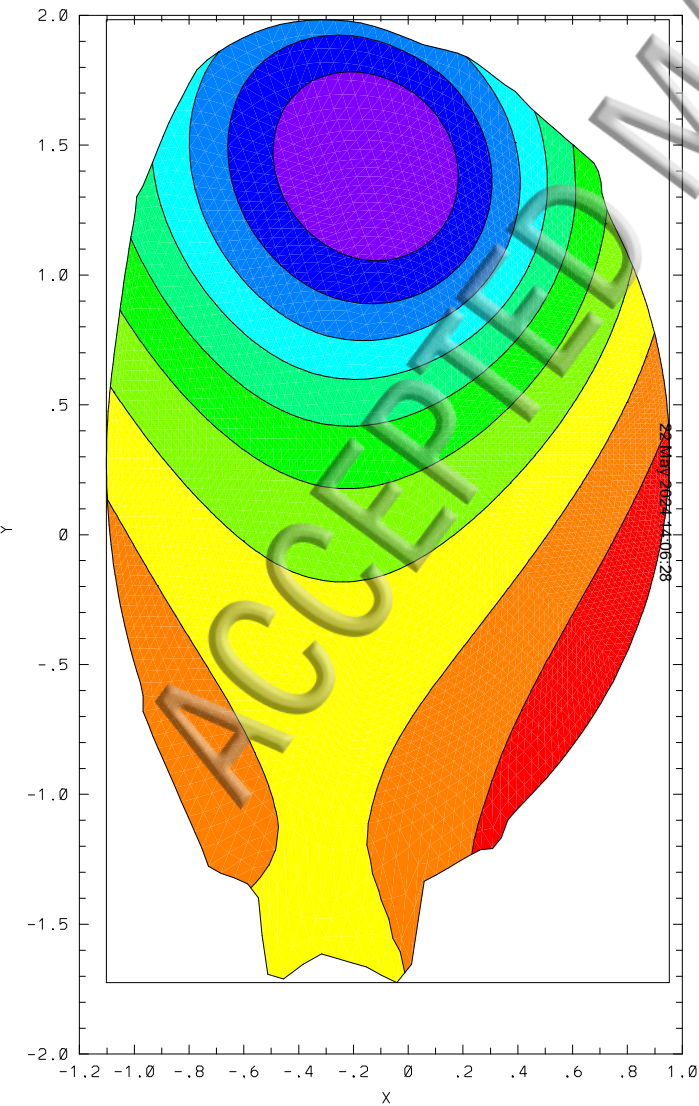


FIG. 9. (a) Peak  $\Delta F_x$  and  $\pi B \Delta M_{IZ}$  as a function of  $\tau_{CQ}/\tau_{wall}$ , with fitting functions. (c) Peak halo fractions  $HF$ ,  $\Delta HF$  as a function of  $\tau_{CQ}/\tau_{wall}$ , with fit.

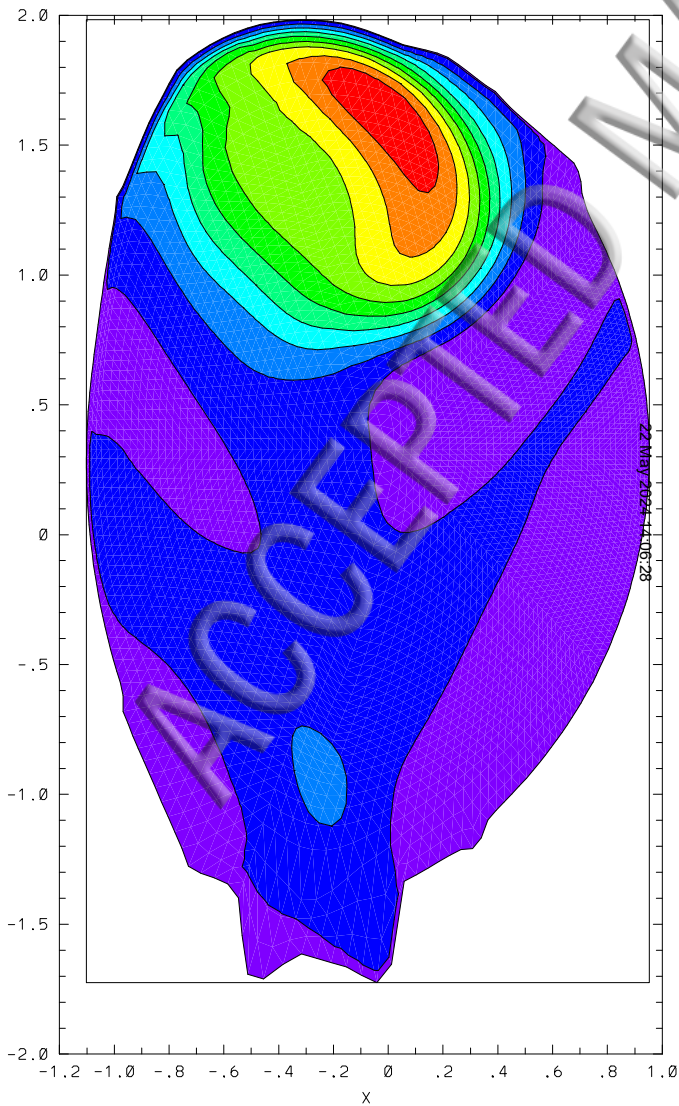




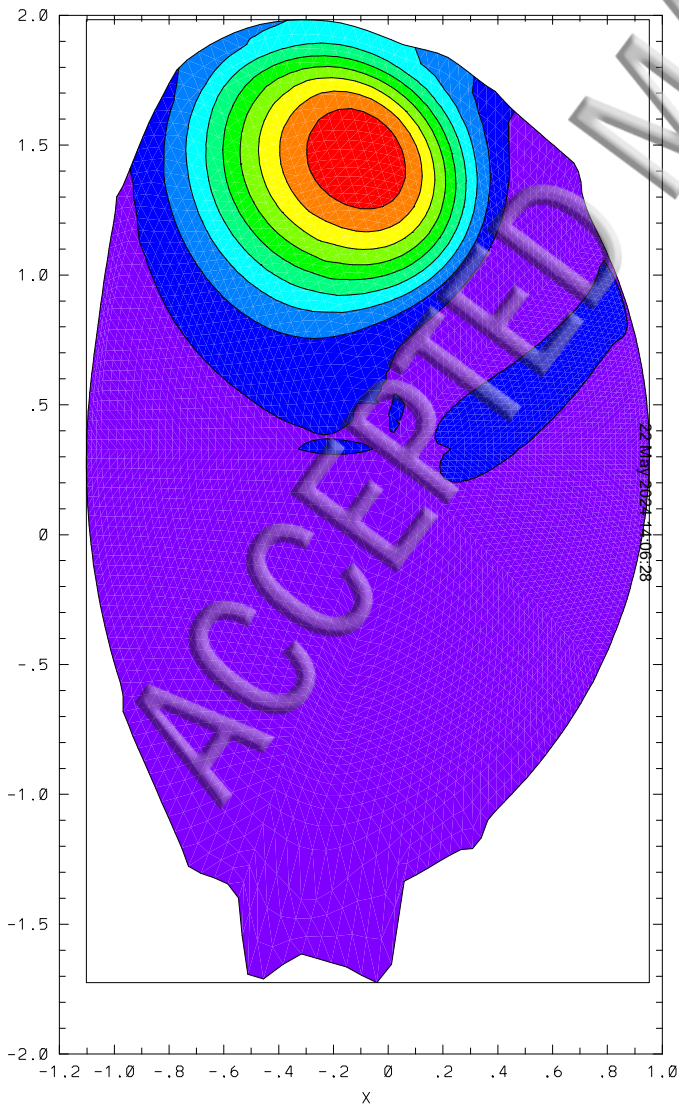
a            max    0.28E+00  
min   -0.48E+00   t= 3925.36



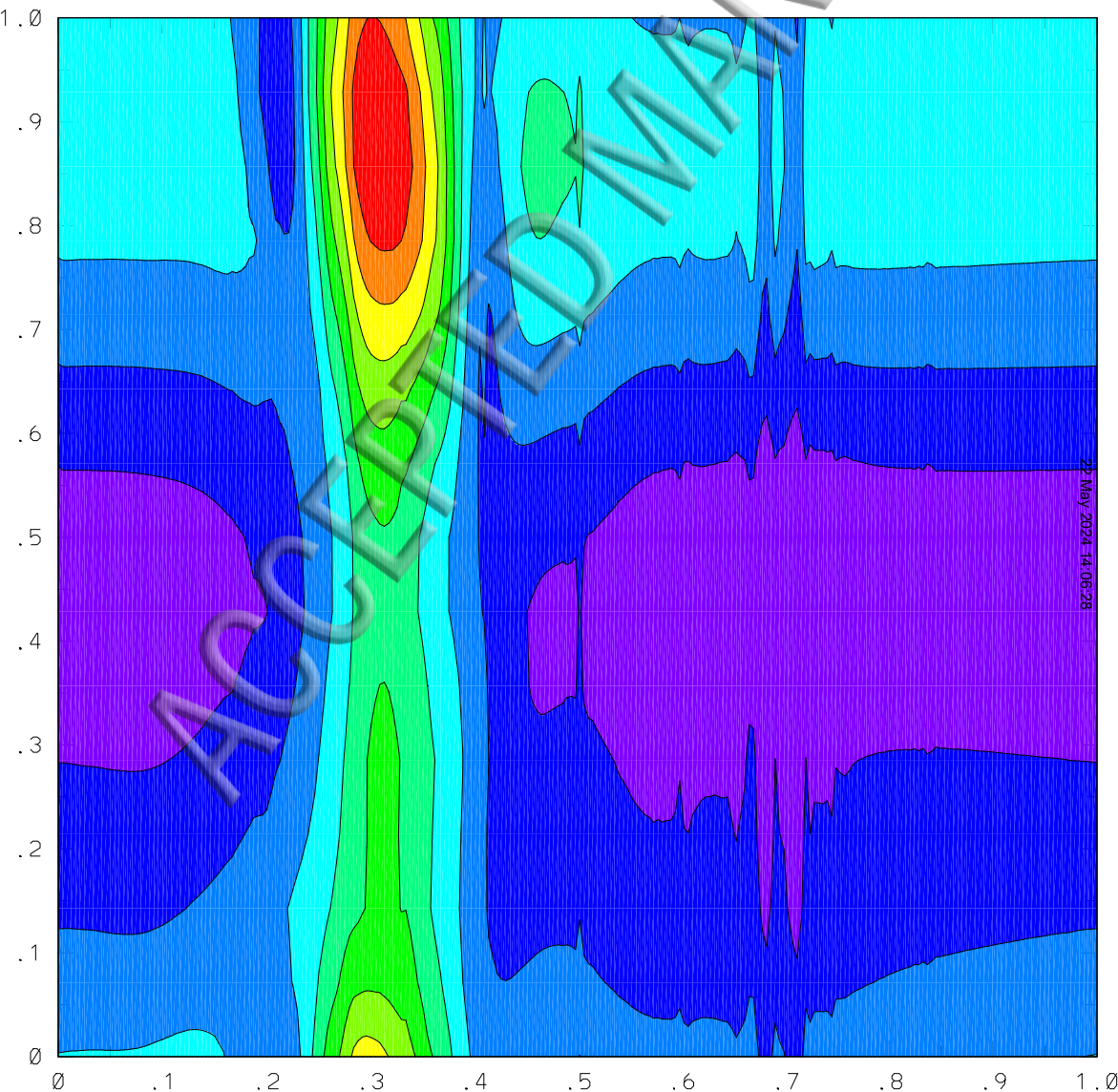
c max 0.34E+01  
min -0.30E+00 t= 3925.36

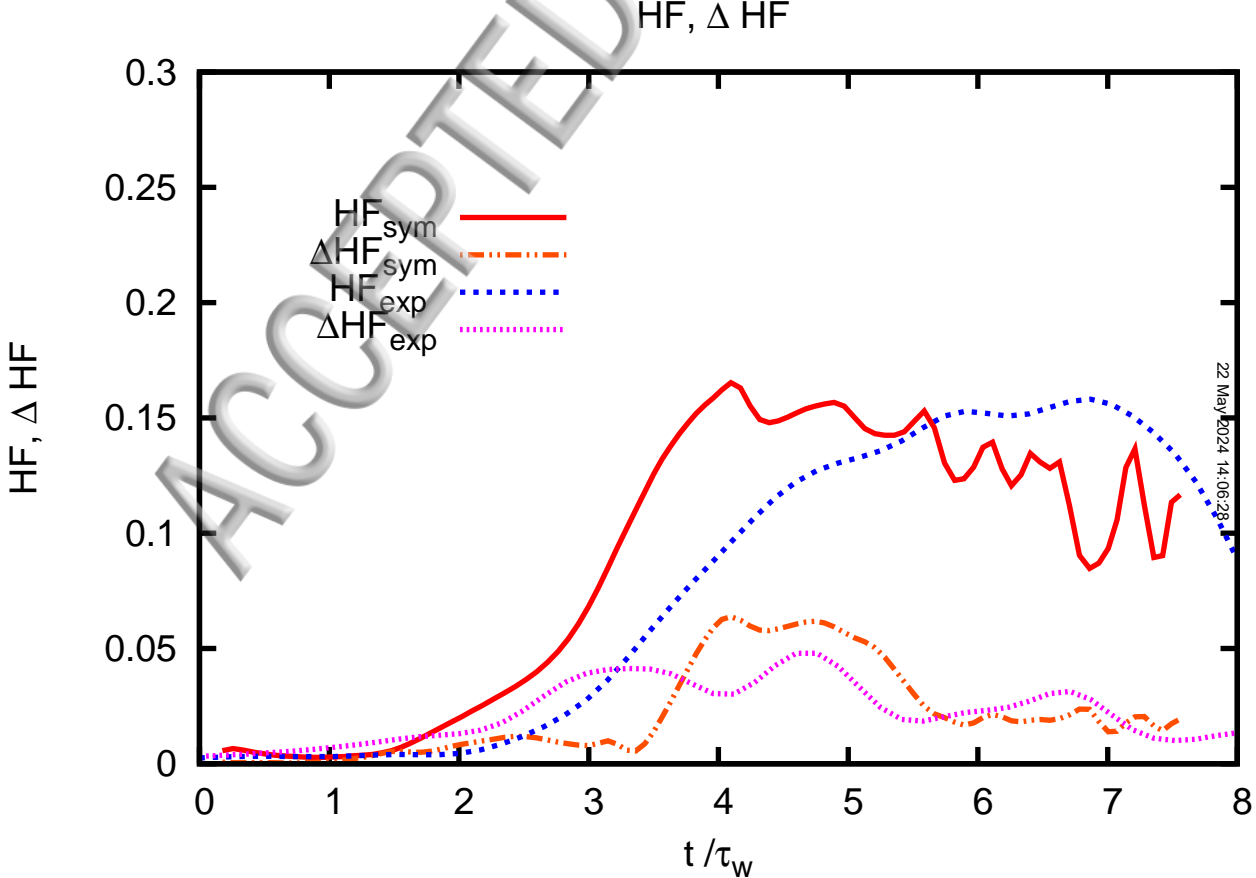


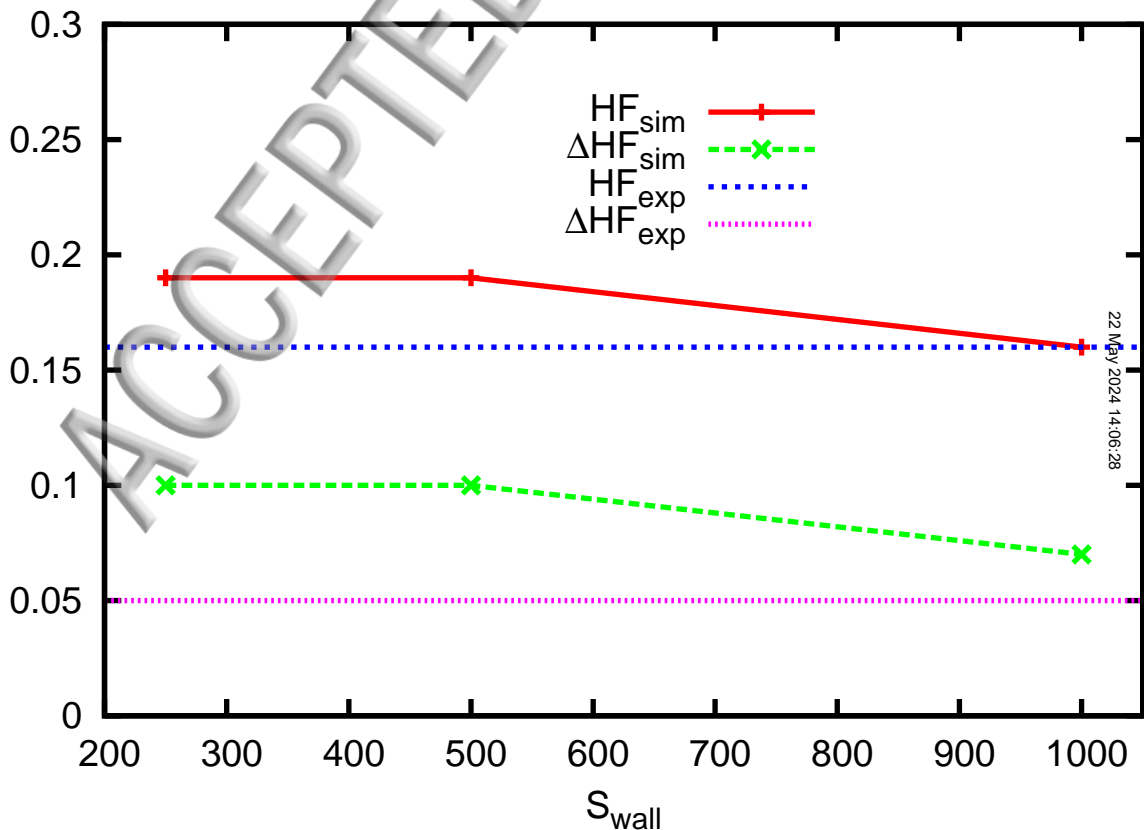
si max 0.18E+00  
min -0.71E-02 t= 3925.36

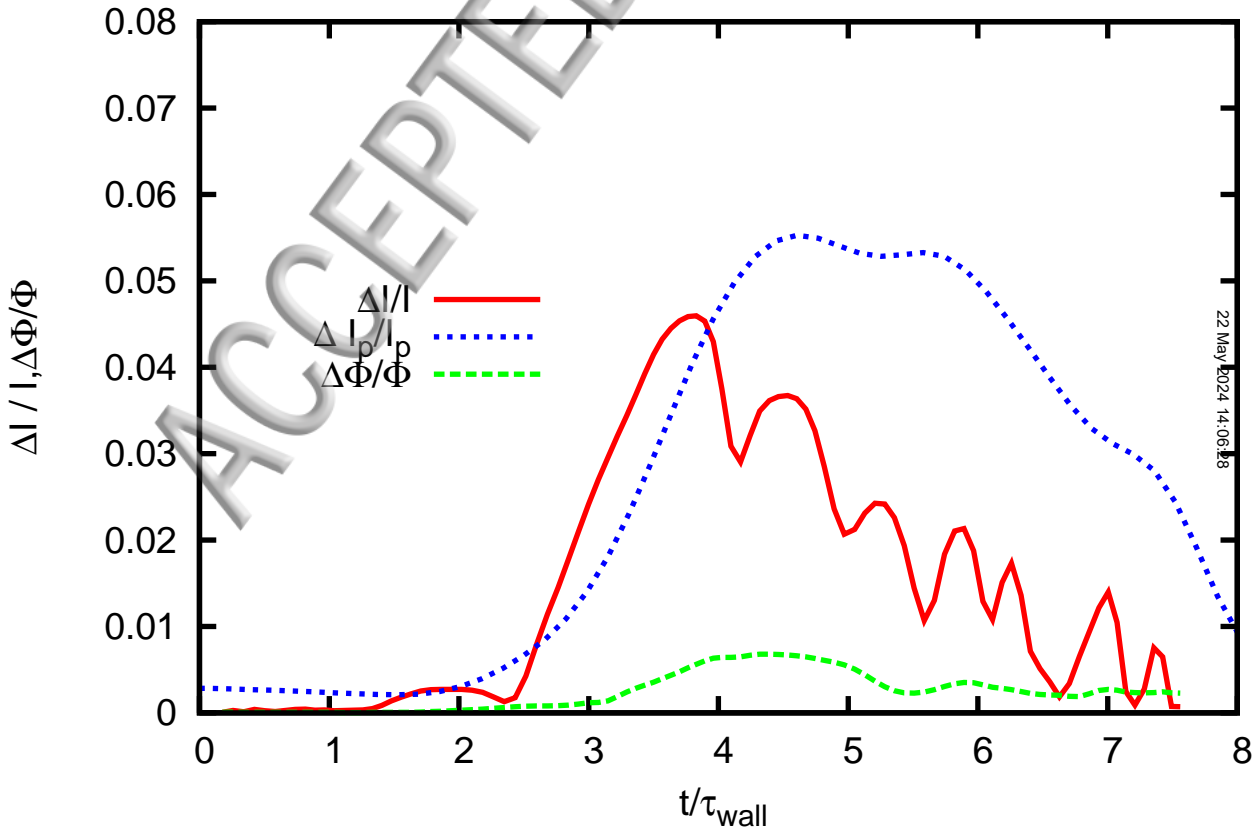


I\_h max 0.50E+00 min -0.17E+00 t= 3925.36

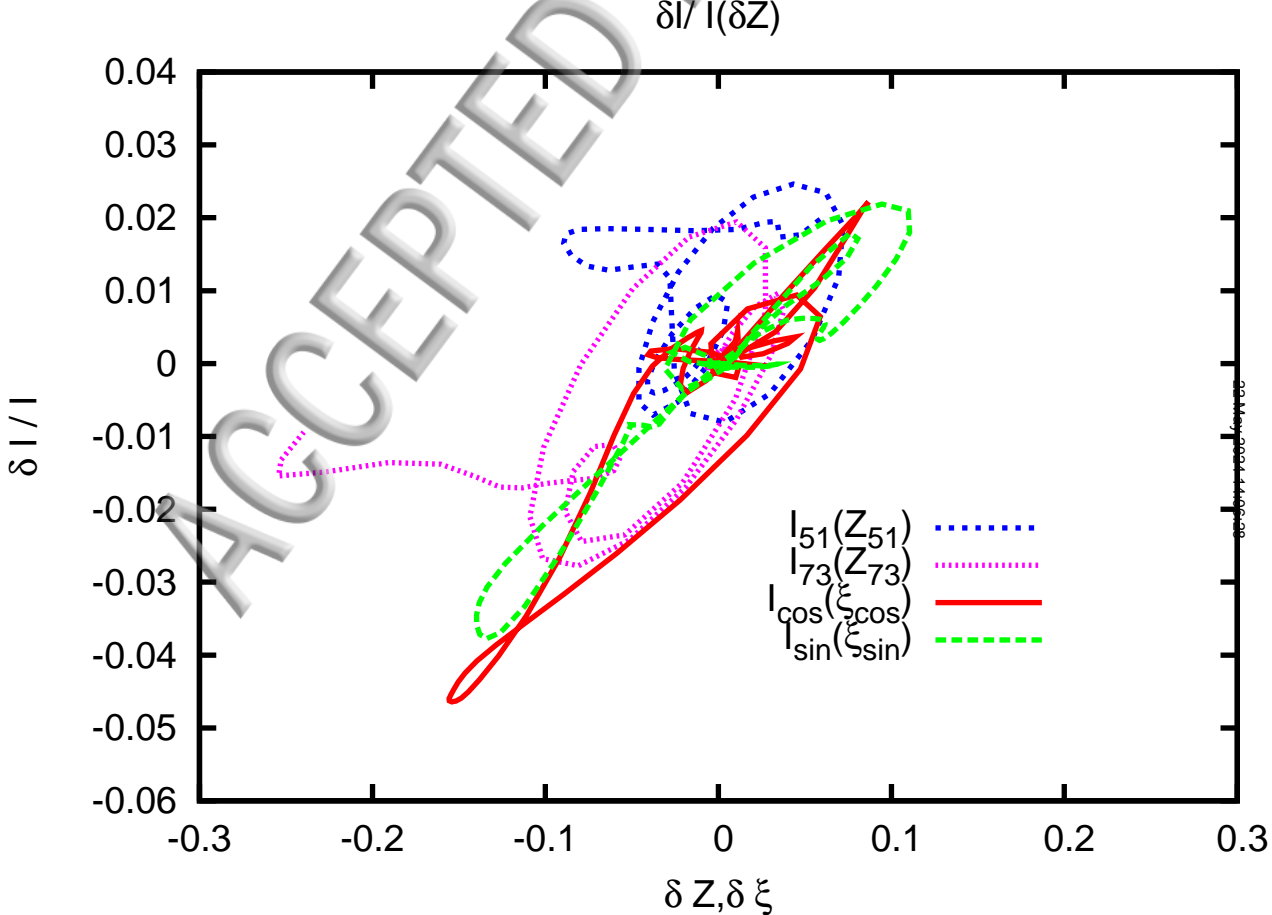


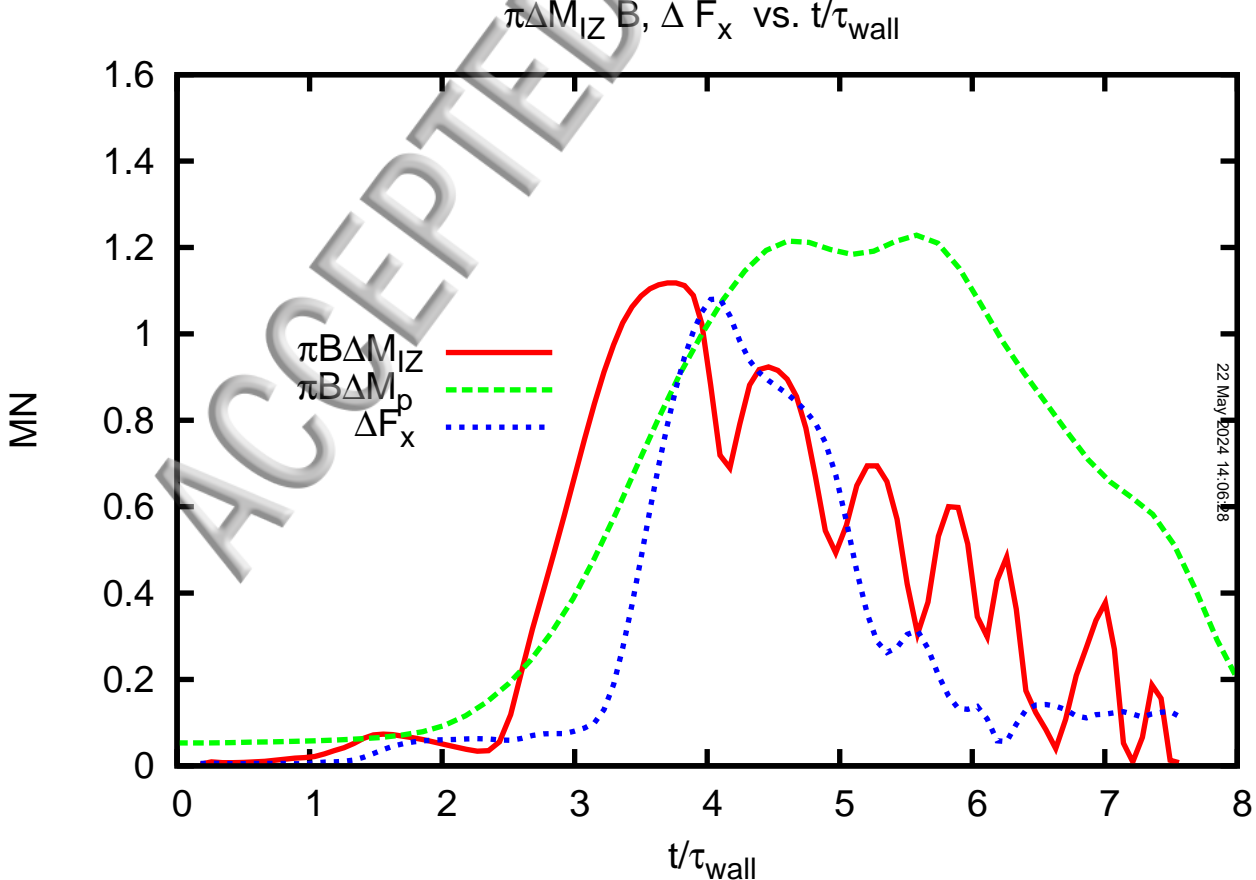


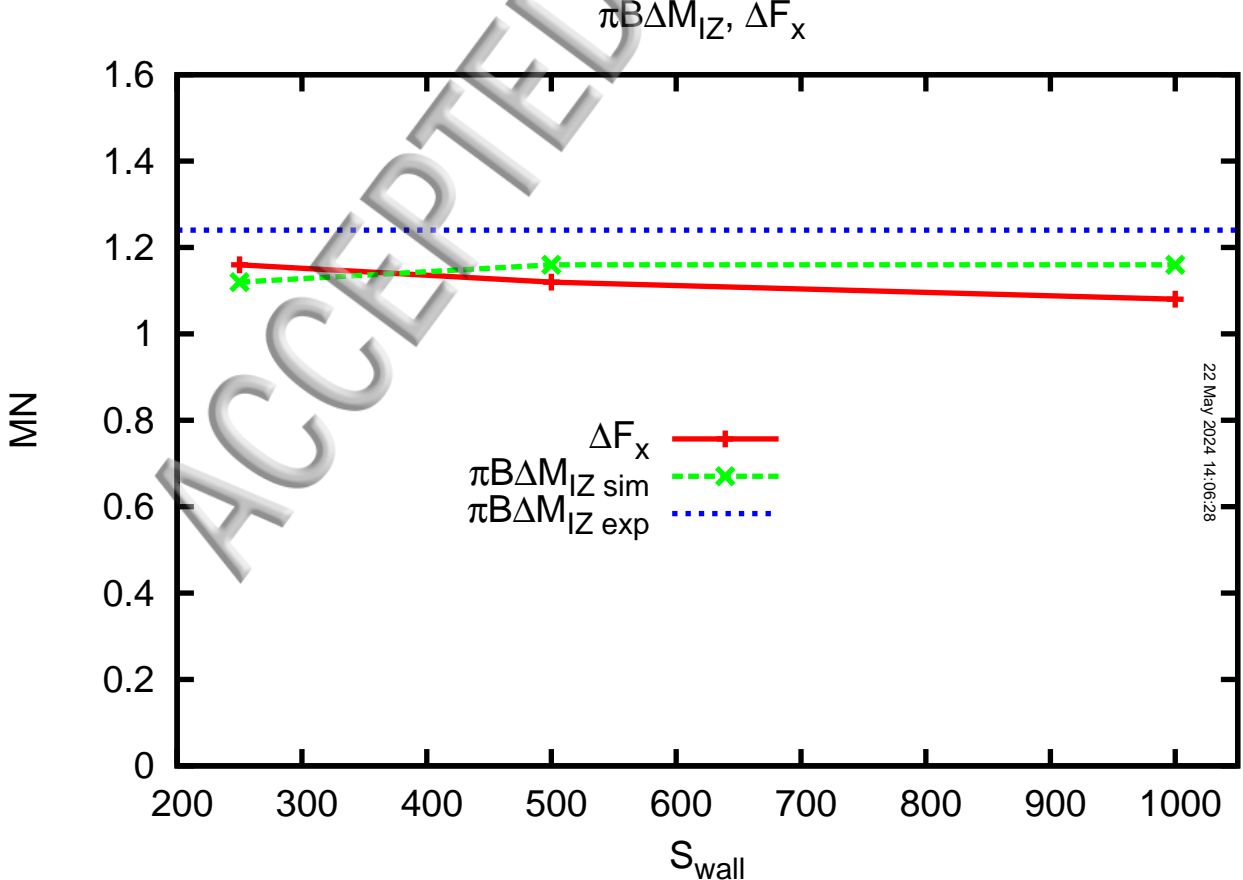


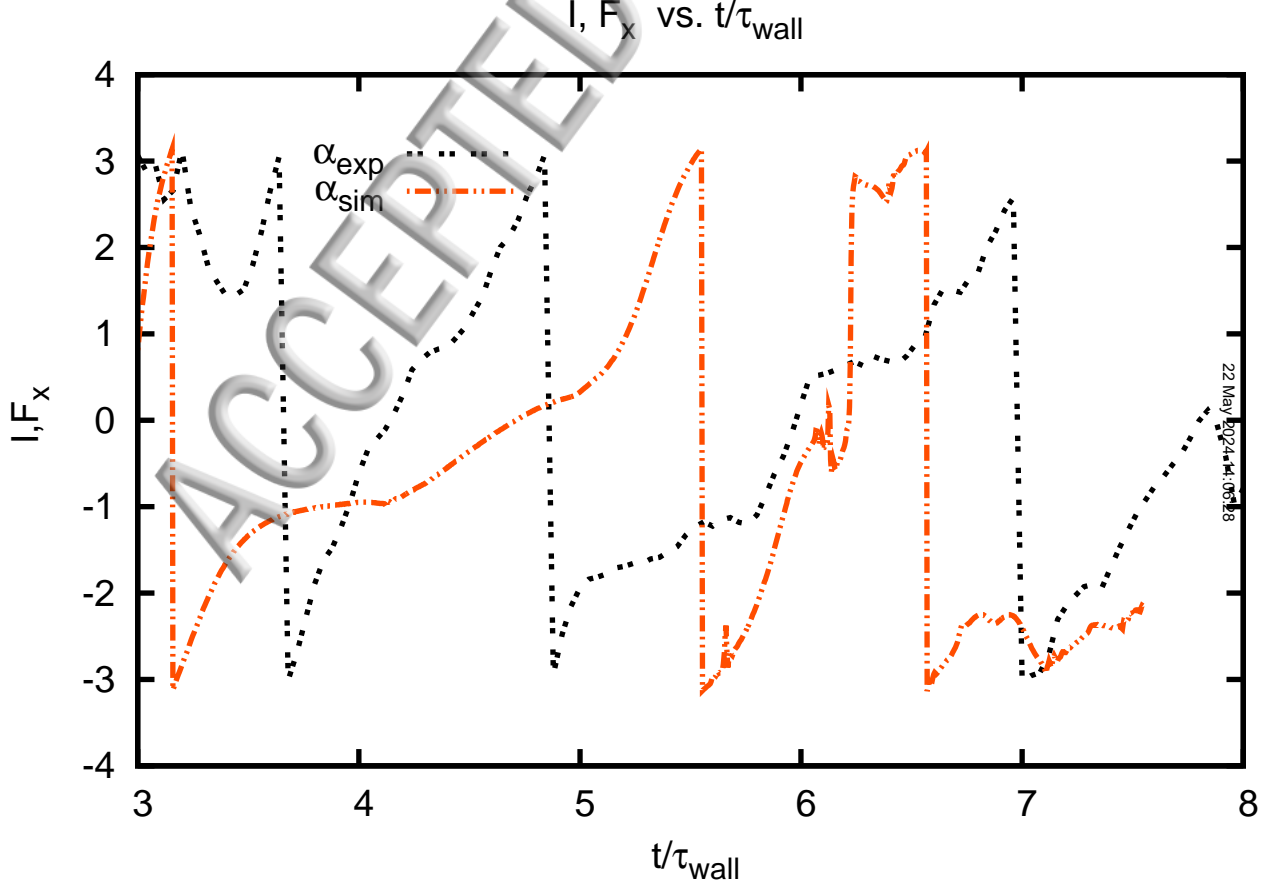




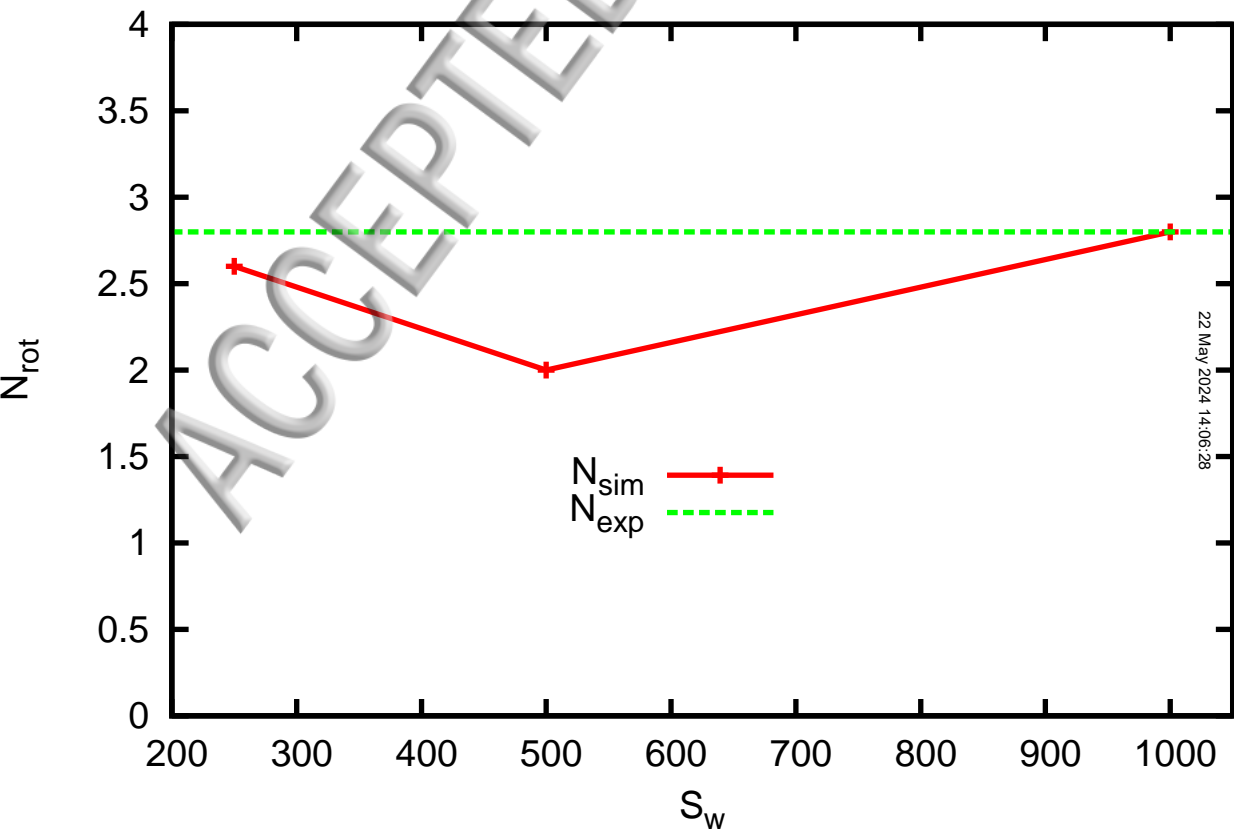


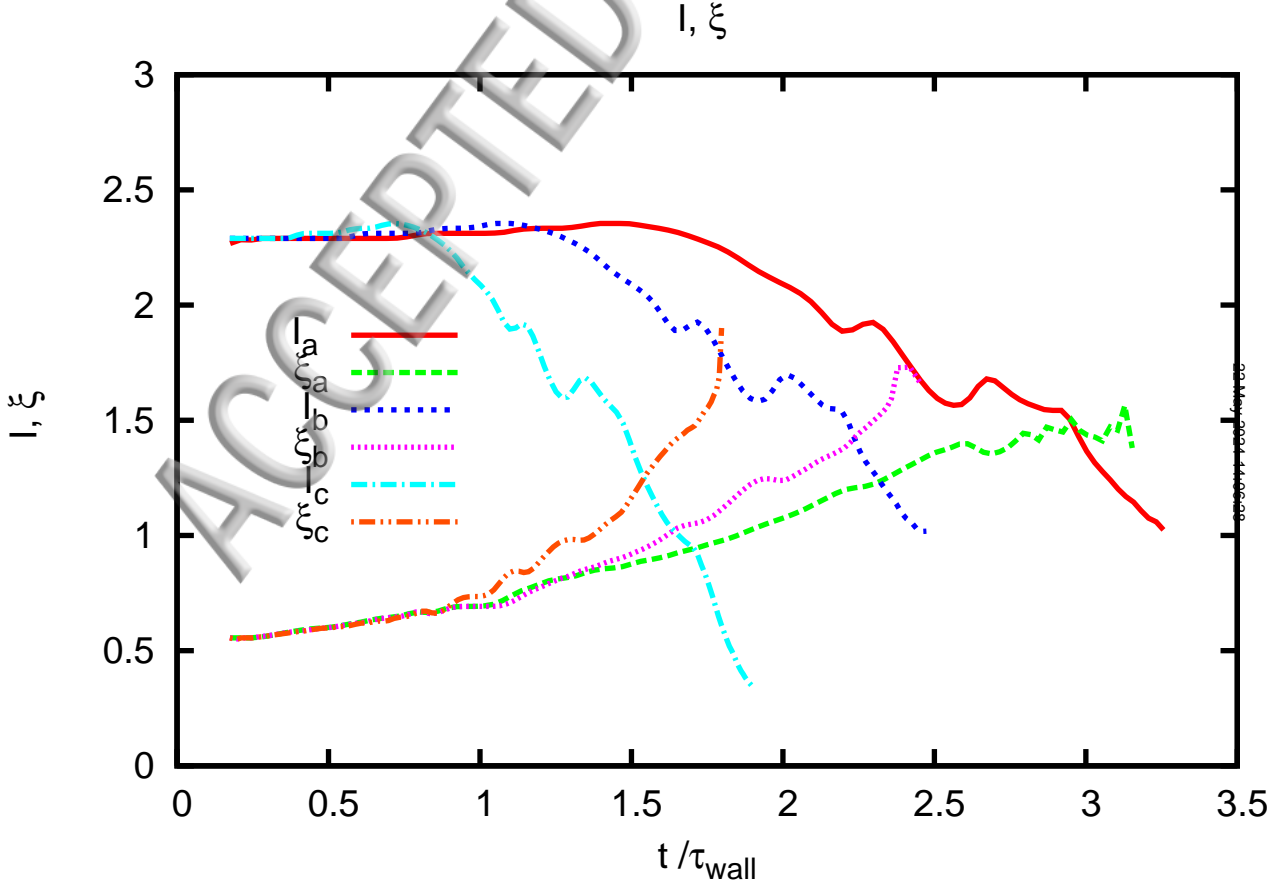






# $N_{\text{rot}}$ vs. $S_w$ in shot 71985





$\Delta F_x$ ,  $\pi B \Delta M_{IZ}$ , vs.  $\tau_{CQ}/\tau_{wall}$

MN

